

The fate of chaotic binaries

Janna Levin

DAMTP, Cambridge University, Wilberforce Rd, Cambridge CB3 0WA

and

The Blackett Laboratory, Imperial College of Science, Technology & Medicine, South Kensington, London SW7 2BZ

e-mail: j.levin@damtp.cam.ac.uk

A typical stellar mass black hole with a lighter companion is shown to succumb to a chaotic precession of the orbital plane. As a result, the optimal candidates for the direct detection of gravitational waves by Earth based interferometers can show irregular modulation of the waveform during the last $\mathcal{O}(30-50)$ orbits. The precession and the subsequent modulation of the gravitational radiation depends on the mass ratio, eccentricity, and spins. The smaller the mass of the companion, the more prominent the effect of the precession. A large eccentricity has less effect on the regularity of the orbit and may even suppress chaotic resonances. The most important parameters are the spin magnitudes and misalignments. If the spins are small and nearly aligned with the orbital angular momentum, then there will be no chaotic precession while increasing both the spin magnitudes and misalignments increases the erratic precession. An irregular precession of the orbital plane will generate irregularities in the gravitational wave frequency but may have a lesser effect on the total number of cycles observed.

04.30.Db,97.60.Lf,97.60.Jd,95.30.Sf,04.70.Bw,05.45

Merging black hole binaries are potent sources of gravitational waves and are among the most promising targets for direct detection by the future interferometric observatories. Black hole mergers, if sufficiently abundant, are likely to be the most common compact binary merger to be detected. If the black holes are rapidly spinning, then the orbit can be extremely irregular, even chaotic, bearing significant implications for gravitational wave searches [1–7]. An earlier *Letter* [2] identified chaos in relativistic, spinning binaries in a somewhat abstract discussion. In this article, the intention is instead to provide a more concrete discussion with less emphasis on formal chaos. What is observationally important is visibly irregular motion. Taking this attitude, a specific astrophysical model is followed through successive stages in order to gauge when irregular motion will occur within the LIGO/VIRGO bandwidth. Specifically, we investigate the orbits of a maximally spinning black hole with a lighter companion.

Certain binary star systems are fated to evolve into black hole binaries. The orbits of these long lived binaries have sufficient time to circularize before entering the LIGO/VIRGO bandwidth as angular momentum is lost to gravitational waves. An archive of circular templates is accruing for various binary parameters. Yet the merger rates of these evolved binaries are predicted to be too low to ensure detection by the first two generations of LIGO detectors. A more promising detection rate is predicted for dynamical binary black holes; that is, binaries formed by the dynamical capture of one black hole by another in dense stellar systems [8]. The merger rate is expected to be about $1.6 \times 10^{-7}/\text{yr}/\text{Mpc}^3$, which exceeds neutron star merger rates as well. Dynamically formed black hole binaries should have a distribution of eccentricities and short orbital periods with masses in the range of $\sim (5-15)M_\odot$ [8]. A binary with masses $m_1 = 15M_\odot$

and $m_2 = 5M_\odot$ for instance will emit gravitational waves with a frequency within the optimal LIGO bandwidth of $f \sim (10-10^2)$ Hz for radial separations $r \sim (50-10)m$ where units of total mass $m = m_1 + m_2$ are used. These provide natural values for the mass and radii ranges to investigate. The heavier black hole is taken to have maximal spin $S_1 = m_1^2$ (spin period $P \sim 3 \times 10^{-4}s$ for a $15M_\odot$ black hole). Unlike pulsars, black holes are expected to essentially maintain the spin they are born with through most of the inspiral. This canonical BH/BH pair can precess chaotically for radii as large as $r \sim 30m$, and perhaps even larger, depending on the orbital parameters.

To verify that the irregular motion is not confined to this one example, a black hole/neutron (BH/NS) star system is also considered. The BH/NS binary is taken to have the typical parameter values of $m_1 = 10M_\odot$ and $m_2 = 1.4M_\odot$. Irregular motion can be seen for radii as large as $r \sim 90m$, or maybe even wider separations, again depending on the orbital parameters. The explosive evolution of stellar progenitors which populate BH/NS pairs delivers large kicks to the objects and leads to large spin misalignments [9]. It is still unclear whether the population of such pairs is too sparse to expect a detection. Since it is only the mass ratio which enters the equations, either of these cases can be scaled to represent the dynamics of much more massive systems which will be visible to LISA [10].

We look for chaotic behaviour when energy is conserved and the radiation reaction is turned off. For an individual orbit, chaos manifests itself as the unpredictable precession of the orbital plane. When considering all possible orbits, chaos manifests itself as an extreme sensitivity of the orbital precession to initial conditions so two neighboring orbits may live out very different precessional histories. The implication is that there is a theoretical limit on how well we can predict the orbit

and therefore the waveform of the emitted gravitational radiation [1,2]. Dissipation from the emission of gravitational waves is then included. Irregular motion in the dissipative system is understood in terms of the number of windings the pair executes in a region of phase space which is chaotic for the underlying conservative system.

The regularity of the orbit will be effected by several parameters: the mass ratio $\beta = m_2/m_1$, the magnitudes of the spins, the spin alignment with respect to the orbital plane, the eccentricity of the orbit, and the radius of the orbit at the time of detection. As is already clear from Ref. [2], motion in the conservative system becomes more irregular the larger the angle the spin makes with the perpendicular to the orbital plane. For all of the examples studied in this article we will take the initial spin angle to be an intermediate value of 45° . The importance of three other parameters is evaluated here: (1) the binary mass ratio $\beta = m_2/m_1$, (2) the magnitude of the second spin \vec{S}_2 , and (3) the eccentricity of the orbit.

The conclusions in brief for the three parameters varied below are the following: (1) The mass ratio primarily effects the cone of precession. The smaller the mass ratio $\beta = m_2/m_1$, the larger the angle subtended by the orbital plane and the larger the modulation of the gravitational waves [11,12]. (2) There can be chaotic motion when the massive black hole spins rapidly even if the companion has no spin. Still, the larger the magnitude of the second spin (and the misalignment), the more irregular the motion. (3) Eccentricity does not substantially enhance chaotic motion. In fact, large eccentricity may suppress chaotic resonances.

II. EQUATIONS OF MOTION AND SPIN PRECESSION

The Post-Newtonian (PN) expansion of the relativistic two body problem leads to a system of equations describing the fate of spinning binaries [13]. The PN expansion converges slowly to the fully relativistic description [14]. For this reason, it is a poor approximation at small separations. Despite its shortcomings, the PN expansion does give the qualitative features of a relativistic system such as nonlinearity, the existence of unstable circular orbits [14], homoclinic orbits [15], and spin precession. Since these are the ingredients for chaotic dynamics, the qualitative behaviour should persist in a more accurate approximation, although the quantitative conclusions are subject to change.

It is worth emphasizing that approximations can introduce chaos when the exact system is truly regular. One might worry that the error at 2PN order has introduced chaos which would be removed if we knew the full equations of motion without approximation. However, the relativistic two-body problem is likely to be more irregular at higher orders as the nonlinearities of general relativity are more accurately represented, not less. One

might even be inclined to take the extreme resistance of the relativistic two-body problem to solution as evidence, or at least confirmation, of nonintegrability.

The validity of the PN expansion is not questioned further and the equations are treated as a self-contained dynamical system. In the PN scheme, the orbit evolves according to the force equation

$$\ddot{\vec{r}} = \vec{a}_{\text{PN}} + \vec{a}_{\text{SO}} + \vec{a}_{\text{SS}} + \vec{a}_{\text{RR}} \quad (2.1)$$

in center of mass harmonic coordinates [12]. The acceleration is due to Post-Newtonian (PN) effects, spin-orbit (SO) and spin-spin (SS) coupling and radiative reaction (RR). The explicit form of \vec{a} can be found in the appendix. The spins also precess due to the relativistic frame dragging and Lens-Thirring effect. The precession equations are

$$\dot{\vec{S}}_1 = \vec{\Omega}_1 \times \vec{S}_1 \quad , \quad \dot{\vec{S}}_2 = \vec{\Omega}_2 \times \vec{S}_2 \quad (2.2)$$

with

$$\vec{\Omega}_1 = \frac{1}{r^3} \left[\left(2 + \frac{3m_2}{2m_1} \right) \vec{L}_N - \vec{S}_2 + 3(\hat{n} \cdot \vec{S}_2)\hat{n} \right], \quad (2.3)$$

and

$$\vec{\Omega}_2 = \frac{1}{r^3} \left[\left(2 + \frac{3m_1}{2m_2} \right) \vec{L}_N - \vec{S}_1 + 3(\hat{n} \cdot \vec{S}_1)\hat{n} \right]. \quad (2.4)$$

The spins precess with constant magnitude although the total spin $\vec{S} = \vec{S}_1 + \vec{S}_2$ may not have constant magnitude.

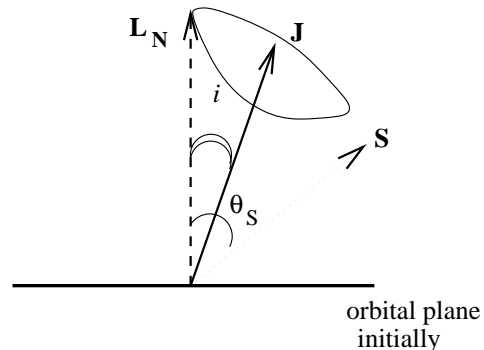


FIG. 1. A schematic drawing of the inclination angle $i = \arccos(\hat{\mathbf{L}}_N \cdot \hat{\mathbf{J}})$ and the angle $\theta_S = \arccos(\hat{\mathbf{L}}_N \cdot \hat{\mathbf{S}})$. The orbital plane traces out a band as in figs. 2 and 3 as the Newtonian angular momentum precesses about \vec{J} .

The orientation of the orbital plane is defined by the Newtonian orbital angular momentum

$$\vec{L}_N \equiv \mu(\vec{r} \times \vec{v}) \quad (2.5)$$

with the reduced mass $\mu = m_1 m_2 / m$ and the total mass $m = m_1 + m_2$. Spin precession, generates a precession of the orbital plane (fig. 1). This can most easily be seen by

noting that to 2PN-order the total angular momentum \vec{J} is conserved with $\vec{J} = \vec{L} + \vec{S}$. The orbital angular momentum \vec{L} can be split into two pieces, $\vec{L} = \alpha\vec{L}_N + \vec{L}_{SO}$ as in eqns. (A15) and (A19). The term \vec{L}_{SO} is due to spin-orbit coupling and α contains Post-Newtonian corrections. To 2PN order $\dot{\vec{J}} = 0$ and so

$$\dot{\vec{L}} \sim -\dot{\vec{S}}. \quad (2.6)$$

The magnitude of the orbital angular momentum is *not* constant. Further, the precession of the orbital plane can be much more complicated than the precession of \vec{S} : $(\alpha\vec{L}_N) \sim -\dot{\vec{S}} - \dot{\vec{L}}_{SO}$. The orbital plane therefore does not just carve out a simple cone as it precesses around the direction of \vec{J} . Instead the plane tilts back and forth as it precesses. The motion becomes chaotic as the tilting back and forth becomes highly irregular in the Hamiltonian system. When radiation reaction is included, the degree of irregularity in the precession of the orbital plane can be estimated in terms of how many windings the pair spends near the chaotic region of the underlying conservative system.

Fig. 2 shows an example of the trajectory for the center of mass of a BH/NS pair. The motion is plotted in three-dimensions to illustrate the precession of the orbital plane.

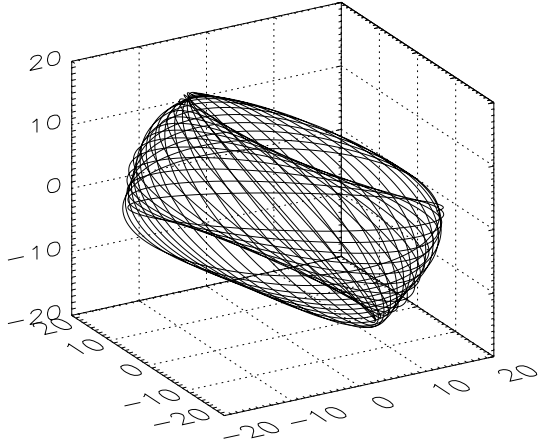


FIG. 2. A three-dimensional view of an orbit with $\beta = m_2/m_1 = 1.4/10$, $S_1 = m_1^2$ and $S_2 = 0$. The initial angle $\theta_1 = \arccos(\vec{L}_N \cdot \vec{S}_1) = 45^\circ$. The initial conditions for the orbit are $r/m = 20$ and $r\dot{\phi} = 0.209$.

The precession, whether regular or irregular, modulates the emitted gravitational waves. The response of a detector on Earth to an impinging gravitational wave can be parametrized as

$$h = F_+ h_+ + F_\times h_\times \quad (2.7)$$

where h_+ and h_\times are the two gravitational wave polarization states and F_+ and F_\times are the antenna patterns. A radiation coordinate system can be defined such that the polarization axes are fixed even in the presence of precession [16]. In such a coordinate system, F_+ and F_\times are constant. However, the polarization states h_+ and h_\times depend on the inclination of the orbit and the precessional frequency in a complicated way [12]. For a circular orbit, the detector response can be written

$$h = A \cos(2\Phi - \delta), \quad (2.8)$$

where the higher harmonics have been ignored for simplicity. The amplitude A and polarization phase δ depend on the binary's location, orientation, and precession [11,12]. For an elliptical orbit, h has terms of the form $\cos(\Phi)$, $\cos(2\Phi)$, and $\cos(3\Phi)$, at quadrupole order so the gravitational wave spectrum shows oscillations at once, twice and three times the orbital frequency.

Precession of the orbital plane will (1) modulate the amplitude in eqn. (2.8) (2) modulate the polarization phase δ and therefore the frequency of the gravitational waves and (3) contribute to the overall accumulated phase by changing the inspiral lifetime. Any extreme sensitivity to initial conditions will most likely have the largest effect on the modulation of the amplitude and frequency of the gravitational waves. The overall accumulated contribution to the number of cycles in the observed waveform will certainly be effected by the general bulk precession but may be less sensitive to the irregularity of the precession until the very final stages of coalescence. The reason for this is that at the radii accessible to the interferometers, the irregularity seems to predominately effect the orientation of the orbit with a lesser effect on the net orbital velocity $\vec{\omega} = \dot{\theta}\hat{\theta} + \sin\theta\dot{\phi}\hat{\phi}$. LIGO/VIRGO aim to observe gravitational waves by accurately measuring the accumulated phase defined as

$$\Psi = \int \omega dt = \int \frac{\omega}{\dot{\omega}} d\omega, \quad (2.9)$$

which may only have a small correction from the irregularity of the precession. Irregular motion will effect the phasing, that is the gravitational wave frequency, and the amplitude of the wave. The number of cycles in the accumulated phase may therefore be determined by the average bulk behaviour of the precession. Although this conjecture requires further scrutiny, we can use the approximations of Refs. [11,12] to provide a rough figure for the number of wave cycles. In Ref. [11], circular Newtonian orbits were studied. The effect of spin precession was isolated without including spin-orbit acceleration terms in the equations of motion in Ref. [11]. This separation of the spin precession equations and the equations of motion removed any possibility of chaotic coupling. However, the gross features can be fairly represented by this approach. They estimate that the change in the total number of cycles amounts to about twice the total number of precessions. For the binary black holes of size

$15M_{\odot} + 5M_{\odot}$, there can be $\sim 10 - 15$ precessions in the observable band and so there can be $\sim 20 - 30$ additional cycles (depending on spin orientation, magnitude and eccentricity of the orbit). In Ref. [12], the contribution to the total number of orbits over the entire LIGO bandwidth was also estimated to be $\sim \mathcal{O}(20)$ for black hole binaries with total mass $\sim 20M_{\odot}$. The number of additional cycles could quadruple for NS/NS masses [12]

It has been argued that matched filtering will be a poor means by which to observe BH/BH orbits in the chaotic regime [2,17] and that other cruder methods will be employed. We contribute to this debate only by indicating when irregularity will influence detectability. It has also been emphasized in Ref. [17], that the PN expansion is not sufficient to accurately model templates for $r \lesssim 15m$. Nonetheless, the higher order contributions will incorporate stronger relativistic effects and therefore more nonlinearity which should only lead to more irregular motion. Since we are trying to provide a physical picture of the general trends and dependences, we continue to use the PN expansion.

III. CHAOS

Chaos in relativistic systems is notoriously difficult to quantify [18,19]. While formal definitions of chaos are of little interest to data analysts when irregularity regardless poses a hindrance, the tools of chaos are nonetheless critical to survey the system for endemic irregularity. In Ref. [2], chaos in the spinning black hole problem was identified through the method of fractal basin boundaries [5,6,2]. In this section we emphasize how to identify irregular motion in an individual orbit. The equations of motion and spin precession equations are treated as any other dynamical system. In the first instance radiation reaction is omitted and chaos is handled in the conservative system. Dissipation is treated in §VII. The 2PN equations of motion can be derived from a Lagrangian [20,21] and therefore can be derived from a Hamiltonian. The coordinates $\vec{S}_1(t)$ and $\vec{S}_2(t)$ can be treated as external time-dependent perturbations to the integrable system with the equations of motion supplemented by the precession eqns. (2.2). The system can therefore be treated as a time-dependent Hamiltonian system $H(\vec{r}, \vec{v}, \vec{S}_1(t), \vec{S}_2(t))$.

Chaos is well defined for Hamiltonian systems. Chaos is synonymous with nonintegrability. Regularity is synonymous with integrability. In a Hamiltonian system with N degrees of freedom q and N conjugate momenta p , integrability prevails when there are N independent constants of the motion. The constants of motion must also be in involution; that is, the Poisson bracket of any constant with the others vanishes: $[C_i, C_j] = 0$. The $2N$ -dimensional phase space can then be reduced to motion on an N -dimensional torus. This is most easily represented with a canonical change of coordinates to action

angle variables (I, Θ) such that each of the N momenta I is set equal to one of the N constants of motion C . The motion can then be made periodic in the coordinate variable Θ . For $N = 1$, degree of freedom, the motion lies on a circle. For $N = 2$, the motion lies on a torus and for arbitrary N , the motion lies on an N -dimensional torus [22,23]. In any other set of canonical variables besides action angle variables, the mark of integrability is that the motion is confined to a smooth closed curve in (p, q) and does not diffuse off that line. If the motion in (r, \dot{r}) has diffused off of a smooth line it is not restricted to a torus and the motion must be nonintegrable.

For coalescing binaries, there are $N = 3$ degrees of freedom, (r, θ, ϕ) . When there are no spins, the phase space is $2N = 6$ -dimensional. The energy and angular momenta provide enough constants of the motion to restrict the trajectories to tori and there is no chaos to 2PN order [2,15]. Beyond 2PN order on the other hand, the two-body problem is likely to be chaotic even in the absence of spin.

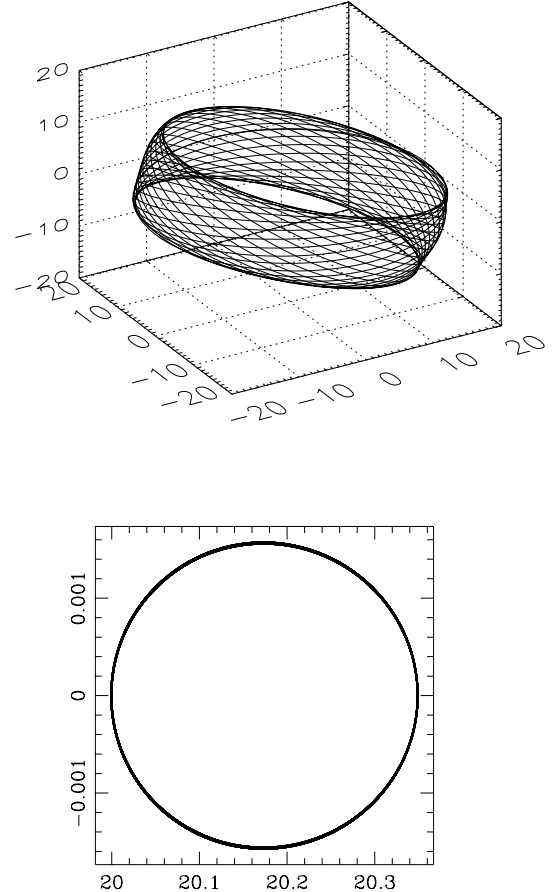


FIG. 3. An orbit with $\beta = m_2/m_1 = 1/3$, $S_1 = m_1^2$ and $S_2 = 0$. The initial angle $\theta_1 = \arccos(\hat{\mathbf{L}}_{\mathbf{N}} \cdot \hat{\mathbf{S}}_1) = 45^\circ$. The initial conditions for the orbit are $r/m = 20$ and $r\dot{\phi} = 0.209$. Top: three-dimensional view of the orbit. Middle: a projection of the orbit onto the (r, \dot{r}) plane.

When the bodies spin, the dynamics can be reduced to a time-independent Hamiltonian system by taking a Poincaré surface of section. The Poincaré surface of section involves plotting a point in (r, \dot{r}) each time the orbit crosses a surface on which all of the other coordinates are fixed. If the collection of points defines a smooth curve, then the motion is confined to a torus and is integrable. If the points speckle the plane, then the motion has diffused off of a torus and is nonintegrable. The Poincaré reduction of phase space is most easily demonstrated for the case of only one spinning body so that $\vec{S} = \vec{S}_1$. Including spin, the phase space is $2N + 3 = 9$ dimensional. The 4 constants of motion, E, \vec{J} , restricts motion to a 5-dimensional surface. If we treat the Hamiltonian as periodic in the three coordinates $\vec{S}(t)$, we can plot a point in (r, \dot{r}) each time the orbit crosses $\vec{S}(t) = \vec{S}(0)$ so that there are only two free coordinates remaining. In this way we can look for the destruction of tori and test for nonintegrability.

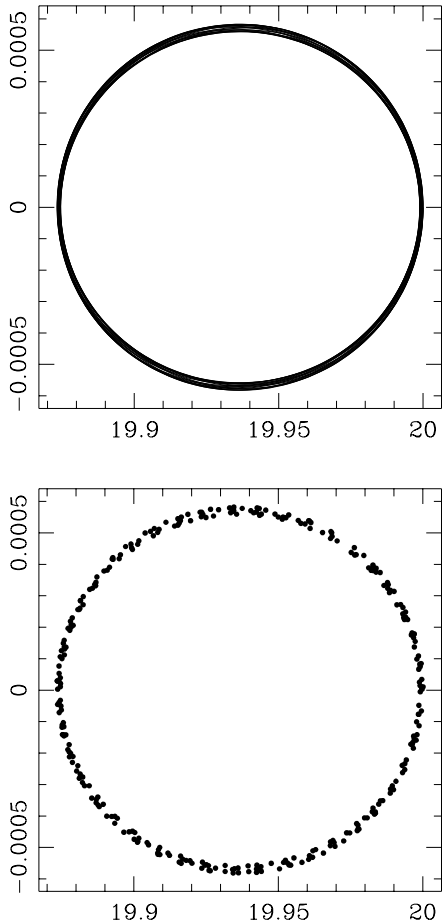


FIG. 4. An orbit with $\beta = m_2/m_1 = 1/3$, $S_1 = m_1^2$ and $S_2 = 0$. The initial angle $\theta_1 = \arccos(\hat{\mathbf{L}}_{\mathbf{N}} \cdot \hat{\mathbf{S}}_1) = 45^\circ$. The initial conditions for the orbit are $r/m = 20$ and $r\dot{\phi} = 0.208$. Top: a projection of the orbit onto the (r, \dot{r}) plane. Bottom: the Poincaré plane obtaining by plotting a point in (r, \dot{r}) each time the spin returns to its initial value.

A BH/BH binary with mass ratio $\beta = m_2/m_1 = 1/3$ is shown in fig. 3. The more massive black hole has spin $S_1 = m_1^2$ with $\arccos(\hat{\mathbf{L}}_{\mathbf{N}} \cdot \hat{\mathbf{S}}_1) = 45^\circ$ initially. The second spin is set to zero for this figure. The topmost panel in fig. 3 shows a three-dimensional view of the orbit. The lower panel shows a projection of the orbit in the (r, \dot{r}) plane. The orbit is very nearly circular. If the orbit is exactly circular with only one spin then there can be no chaos since the dimensionality of the phase space reduces to two [2], which is not enough to support chaos. This orbit is fairly regular although there is some slight spreading in the projection onto the (r, \dot{r}) plane. This spreading becomes more pronounced for a slightly different initial velocity as shown in fig. 4. The top panel is the projected motion in the (r, \dot{r}) plane which shows some threading of the orbit. To confirm unambiguously the destruction of the torus, the Poincaré surface of section is shown in the bottom panel.

In theory, the surface of section technique can also be implemented in the case of two spinning bodies since both are periodic under the precession. In practice this can be difficult since one might have to wait a very long time before $\vec{S}_1(t) = \vec{S}_1(0)$ at the same time as $\vec{S}_2(t) = \vec{S}_2(0)$. We can cheat slightly and simply look at the projection of (r, \dot{r}) in the full phase space without taking a Poincaré section. If the projected motion lies on a simple closed curve, the motion is decidedly integrable. If the motion lies on a threaded orbit (such as that of fig. 6), then this indicates the motion has diffused off of a torus. Although strictly speaking this projection may be ambiguous, none of the cases explicitly checked gave false results. *

IV. THE BINARY MASS RATIO

The binary mass ratio $\beta = m_2/m_1$ primarily effects the cone of precession. The lighter the relative mass of the companion, the larger the band in which the orbital plane will precess and the larger the corresponding modulation of the waveform [11,12]. The orbital plane will precess around \vec{J} with an angle of inclination

$$\cos i = \hat{\mathbf{L}}_{\mathbf{N}} \cdot \hat{\mathbf{J}} = \frac{1 + (S/L_N) \cos \theta_S}{\sqrt{1 + (S/L_N)^2 + 2(S/L_N) \cos \theta_S}} \quad (4.1)$$

where $\cos \theta_S \equiv \hat{\mathbf{L}}_{\mathbf{N}} \cdot \hat{\mathbf{S}}$ as in fig. 1 and the total angular momentum has been used to lowest order, $\hat{\mathbf{J}} \sim \hat{\mathbf{L}}_{\mathbf{N}} + \hat{\mathbf{S}}$.

*A fruitful analytic approach may be to treat the motion as an instance of Arnol'd diffusion [22]. Even if \dot{r} is small and \vec{S} changes slowly, their presence induces a coupling between $\dot{\theta}$ and $\dot{\phi}$ which can lead to chaotic resonances and hence stochastic behaviour. The future direction of this work is to interpret the chaotic motion in terms of this slow modulation diffusion [22].

The angle subtended changes as the angle between $\vec{\mathbf{L}}_{\mathbf{N}}$ and $\vec{\mathbf{S}}$ changes. This leads to the additional tilting back and forth on top of the simple precession. The ratio S/L_N can be estimated by taking $L_N \sim \mu(mr)^{1/2}$ for a nearly circular orbit. Consider the extremes when the more massive object spins with $S_1 = m_1^2$ to get an upper range and the opposite regime when the lighter star spins with $S_2 = m_2^2$ to get a lower range:

$$\left(\frac{m_2}{m_1}\right)(m/r)^{1/2} \leq \frac{S}{L_N} \leq \left(\frac{m_1}{m_2}\right)(m/r)^{1/2} \quad (4.2)$$

For very small S/L_N , the precession cone angle is so tight that modulations of the gravitational wave signal will not be substantial. Notice from the left-hand side of eqn. (4.2) that if only the lighter object spins then S/L_N is small for all r . This may explain why Ref. [1] found chaos for a test particle around a Schwarzschild black hole only if the light companion had a spin $S_2 > 0.64m_2m_1$ for $m_1 \gg m_2$, which exceeds the maximal spin of $S_2 = m_2^2$. The 2PN expansion to the two-body problem allows both black holes to spin and precess. When the more massive object spins maximally, then S/L_N is large for $m_1 \gg m_2$. For a 10 : 1 mass ratio, $S/L_N \sim 1$ for $r \sim 100m$. As a result, for large mass ratios, the orbital plane subtends a larger angle at a given radius and modulation will be correspondingly larger [11,12]. Consider fig. 2 versus fig. 3. In both figures, the more massive BH spins maximally ($S_1 = m_1^2$) with a spin displacement of $\vec{\mathbf{L}}_{\mathbf{N}} \cdot \vec{\mathbf{S}} = \cos(45^\circ) = 1/\sqrt{2}$. In both figures, the companion has no spin. The difference between the two figures is the mass ratio. In fig. 2, the mass ratio is $\beta = 1.4/10$ and the angle subtended at $r = 20$ is $i \sim 28^\circ$. In fig. 3, the mass ratio is $\beta = 1/3$ and the angle subtended at $r = 20$ is $i \sim 18^\circ$. The band subtended by the precessing plane is larger for the smaller mass ratio, although it is substantial in both cases.

We can invert eqn. (4.1) using the right-hand-side of eqn. (4.2) to write the radius at a given inclination,

$$\left(\frac{r}{m}\right)^{1/2} \sim \left(\frac{m_1}{m_2}\right) \times \left[\frac{\cos^2 i - \cos^2 \theta_1}{\cos \theta_1 (1 - \cos^2 i) + \sqrt{\cos^2 i (1 - \cos^2 i) (1 - \cos^2 \theta_1)}} \right]$$

with $\cos \theta_1 \equiv \vec{\mathbf{L}}_{\mathbf{N}} \cdot \vec{\mathbf{S}}_1$. We could take this as an indicator for the radius at which precession becomes important. Letting $i \sim 15^\circ$ and $\theta_1 \sim 45^\circ$, then

$$\frac{r}{m} \sim 4 \times \left(\frac{m_1}{m_2}\right)^2. \quad (4.3)$$

For circular motion, $L \sim \mu(mr)^{1/2}$ and $m\dot{\phi} \sim (m/r)^{3/2}$ and the frequency of the emitted wave, $f \sim \dot{\phi}/\pi$ is roughly

$$f \sim 9 \times 10^3 \beta^3 \left(\frac{M_\odot}{m}\right) \text{ Hz}. \quad (4.4)$$

For a BH/BH binary with $\beta \sim 1/3$ and $m = 20M_\odot$, then $f \sim \mathcal{O}(10)$ Hz when the spin precession angle opens to $i \sim 15^\circ$ and the effects on the gravitational wave should be noticeable. For a BH/NS binary with $\beta \sim 1.4/10$ and $m = 11.4$, then $f \sim \mathcal{O}(1)$ Hz when the spin precession angle opens to $i \sim 15^\circ$. To emphasize, precession will be important for these and larger frequencies as the pairs sweep through the interferometer's bandwidth.

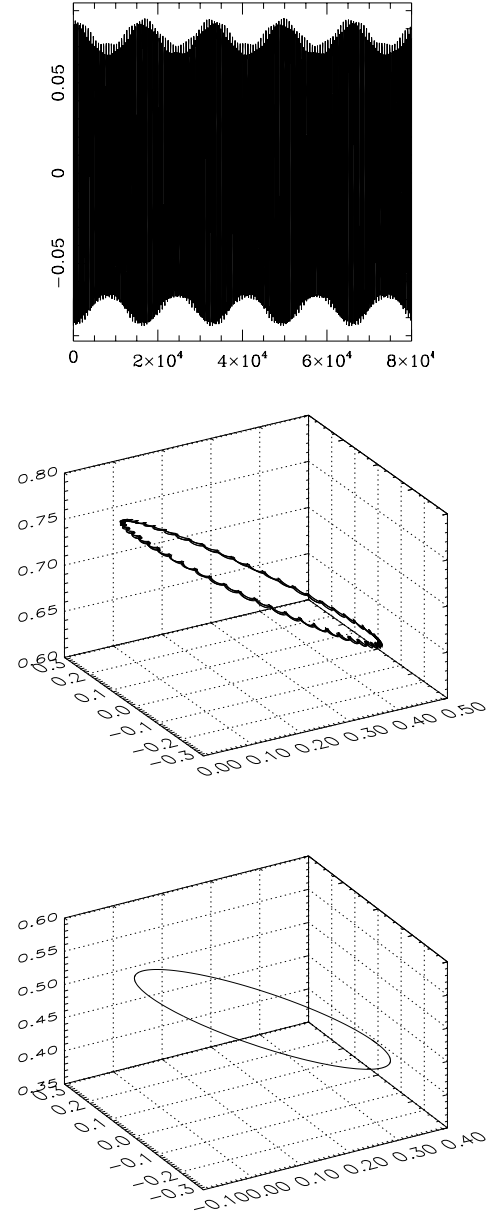


FIG. 5. The waveform, Newtonian angular momentum and spin for the orbit of fig. 3. Top: The waveform h_+ . Middle: three-dimensional view of $\vec{\mathbf{L}}_{\mathbf{N}}$. Bottom: three-dimensional view of the precession of $\vec{\mathbf{S}}_1$.

While we can conclude that smaller mass ratio means a wider precessional angle, the dependence of the reg-

ularity of the motion on β within that band is not yet clear. Within the bulk precession, the orbital plane tilts back and forth, sometimes regularly and sometimes erratically. Orbits can subtend roughly the same cone but some occupy the band more regularly than others. A hint of the effect of β on regularity comes from a comparison of frequencies. An instantaneous orbital frequency can be defined roughly as

$$\omega \sim \frac{L_N}{\mu r^2} \quad (4.5)$$

for comparison with the instantaneous spin precession frequency of the larger object (neglecting spin-spin coupling just for the crude estimate)

$$\Omega_1 \sim \left(2 + \frac{3m_2}{2m_1}\right) \frac{L_N}{r^3} \quad (4.6)$$

so that

$$\frac{\omega}{\Omega_1} \simeq \frac{(\beta + 1)^2}{\beta(2 + 3\beta/2)} \left(\frac{r}{m}\right). \quad (4.7)$$

Therefore ω/Ω_1 is always large. The pair executes many orbital windings per spin precession. This hints that the chaotic behaviour may be related to modulation diffusion where a slowly varying parameter, in this case $\tilde{\mathbf{S}}_1$, facilitates chaotic resonances between coordinates, in this case θ and ϕ [22].

However, compared to the instantaneous precession frequency of the spin of the lighter object

$$\frac{\omega}{\Omega_2} \simeq \frac{(\beta + 1)^2}{(2\beta + 3/2)} \left(\frac{r}{m}\right). \quad (4.8)$$

This ratio is not as large for small β so the lighter companion always precesses much more than the heavy black hole. As argued in §V, the spin of the companion encourages irregularity and the fact that $\Omega_2/\Omega_1 < 1$ may account for some of this effect.

In general, the mass ratio $\beta = m_2/m_1$ seems to effect the bulk shape of the precession and gravitational wave modulation. By eqns. (4.7) and (4.8), β may determine the radii at which chaotic resonances will occur. Still, it is unclear how much the mass ratio impacts the details of the motion.

For comparison with later cases, the waveform emitted by the BH/BH binary of fig. 3 is shown in the top panel of fig. 5. Even though the precession is fairly regular, it does modulate the wave amplitude and frequency. The modulation of the waveform has been minimized by placing the binary directly above the detector. Tail-effects are neglected throughout. A three dimensional view of $\tilde{\mathbf{L}}_N$ is shown in the middle panel of fig. 5. The lower panel shows the precession of the spin $\tilde{\mathbf{S}}_1$.

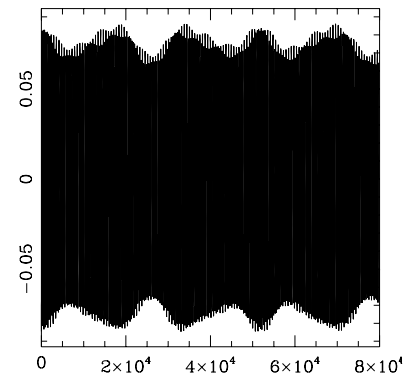
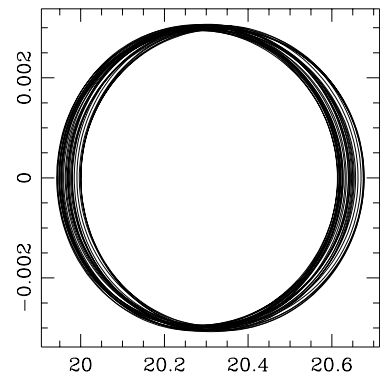
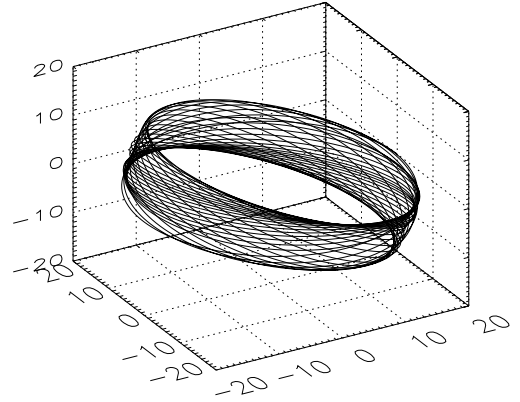


FIG. 6. An orbit with $\beta = m_2/m_1 = 1/3$, $S_1 = m_1^2$ and $S_2 = m_2^2$. The initial angle $\theta_1 = \arccos(\tilde{\mathbf{L}}_N \cdot \tilde{\mathbf{S}}_1) = 45^\circ$. The initial conditions for the orbit are $r/m = 20$ and $r\dot{\phi} = 0.209$. Top: three-dimensional view of the orbit. Middle: a projection of the orbit onto the (r, \dot{r}) plane. Bottom: the waveform.

V. SECOND SPIN

The effect of spinning up the lighter companion can be studied by starting with the regular orbit of fig. 3. Even a second spin as small as $S_2 = 0.05m_2^2$ begins to cause some diffusion in phase space. When the second

spin is maximal, the fraying of the projection in (r, \dot{r}) increases. Fig. 6 shows a three-dimensional orbit, the projected motion in (r, \dot{r}) , and the waveform when both objects spin maximally. Fig. 7 shows the precession of the orbital plane, as well as the precession of both spins.

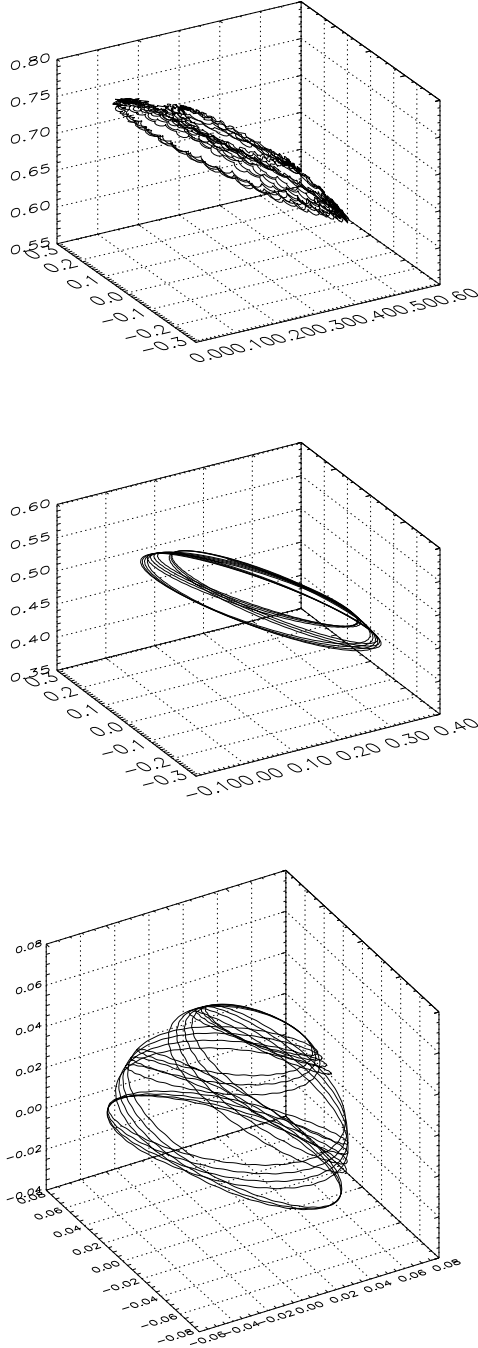


FIG. 7. The Newtonian angular momentum and spins for the orbit of fig. 6. Top: three-dimensional view of \vec{L}_N . Middle: three-dimensional view of the precession of \vec{S}_1 . Bottom: three-dimensional view of the precession of \vec{S}_2 .

The fraying of the orbit in (r, \dot{r}) confirms that the mo-

tion is not confined to a torus. As discussed in §III, this destruction of toroidal motion is the tell tale sign of nointegrability; that is, of chaos. Notice in fig. 7 that the spin of the lighter star precesses more than the spin of the heavier object as expected from eqns. (4.7)-(4.8).

VI. ECCENTRICITY

Binary black holes formed in dense stellar regions are thought to have a roughly thermal distribution in eccentricity with a slight enhancement of high e at the time of formation [8]. While many of these may still have time to circularize before merger, it is worth investigating the role of eccentricity on the regularity of the orbit. Increasing eccentricity does not appear to enhance chaotic motion. Consider fig. 8 where only one of the holes is spinning. The top panel shows the three-dimensional orbit which does have irregular features. However, this is deceptive. It is well known that Keplerian orbits are closed ellipses while relativistic, elliptical orbits precess within the orbital plane. The entire plane then precesses due to the spins. What is being witnessed in the top panel of fig. 8 is this double precession. The middle panel shows complete regularity of the orbit in (r, \dot{r}) . Motion in this coordinate is confined to a torus. The waveform shown in the bottom panel shows several expected features. Since the orbit is elliptical, the gravitational waves oscillate at once, twice and three times the orbital frequency which changes the spectrum from that for a circular orbit. The double precession then modulates the amplitude and phase on top of these oscillations. Even though this motion is regular (for $S_2 = 0$), in the sense of being predictable, the modulation of the waveform from the double precession must certainly impact observations gained through the method of matched filtering.

Eccentric orbits do show chaotic precession when the companion spins rapidly as well. (Note that when both stars spin, there are no circular orbits [12].)

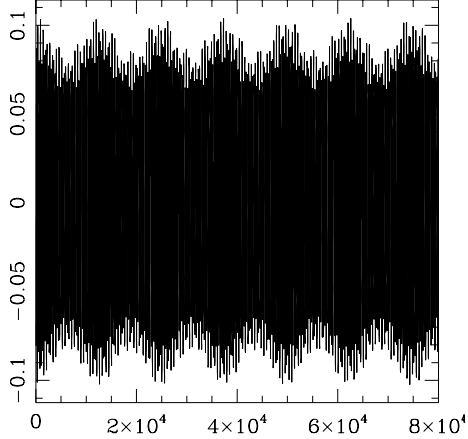
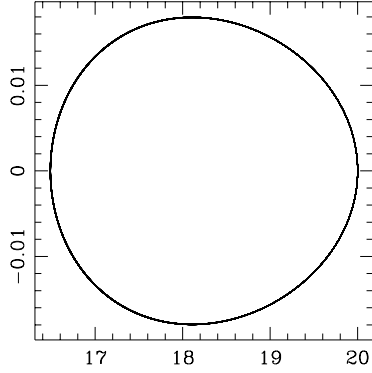
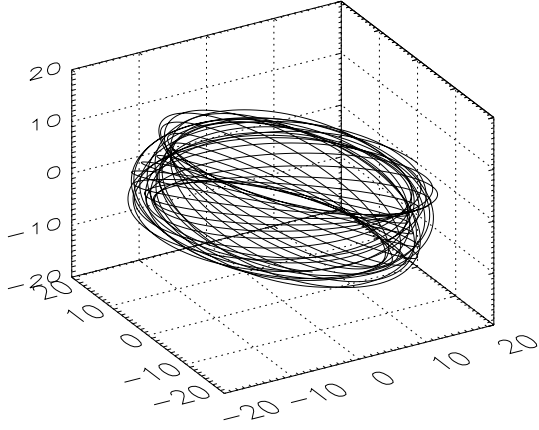


FIG. 8. An orbit with $\beta = m_2/m_1 = 1/3$, $S_1 = m_1^2$ and $S_2 = 0$. The initial angle $\theta_1 = \arccos(\hat{\mathbf{L}}_{\mathbf{N}} \cdot \hat{\mathbf{S}}_1) = 45^\circ$. The initial conditions for the orbit are $r/m = 20$ and $r\dot{\phi} = 0.2$. Top: three-dimensional view of the orbit. Middle: a projection of the orbit onto the (r, \dot{r}) plane. Bottom: the waveform.

Before addressing dissipation, for completeness, a chaotic orbit in the energy conserving system at low radius ($r \sim 10m$) is shown in figs. 9 and 10. As expected, the precession is increasingly erratic as the radial sepa-

ration decreases. The impact of irregularity and unpredictability of the precessing plane will get increasingly more pronounced in the wave form as the pair coalesces.

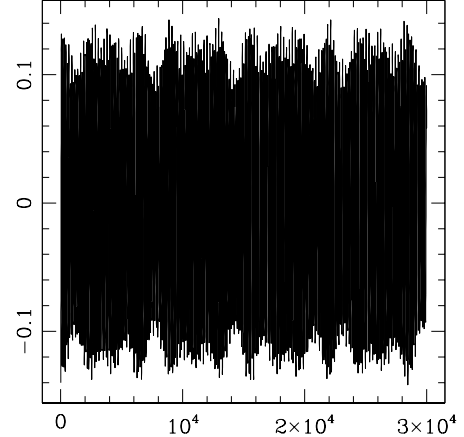
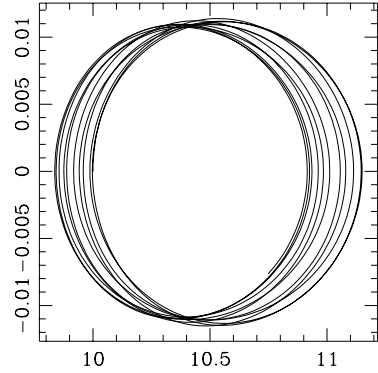
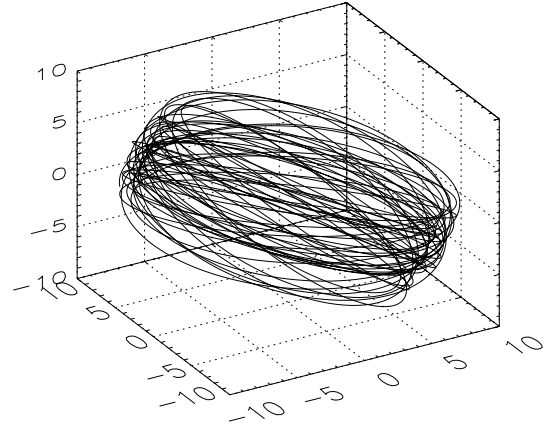


FIG. 9. An orbit with $\beta = m_2/m_1 = 1/3$, $S_1 = m_1^2$ and $S_2 = m_2^2$. The initial angle $\theta_1 = \arccos(\hat{\mathbf{L}}_{\mathbf{N}} \cdot \hat{\mathbf{S}}_1) = 45^\circ$. The initial conditions for the orbit are $r/m = 10$ and $r\dot{\phi} = 0.28$. Top: three-dimensional view of the orbit. Middle: a projection of the orbit onto the (r, \dot{r}) plane. Bottom: the waveform.

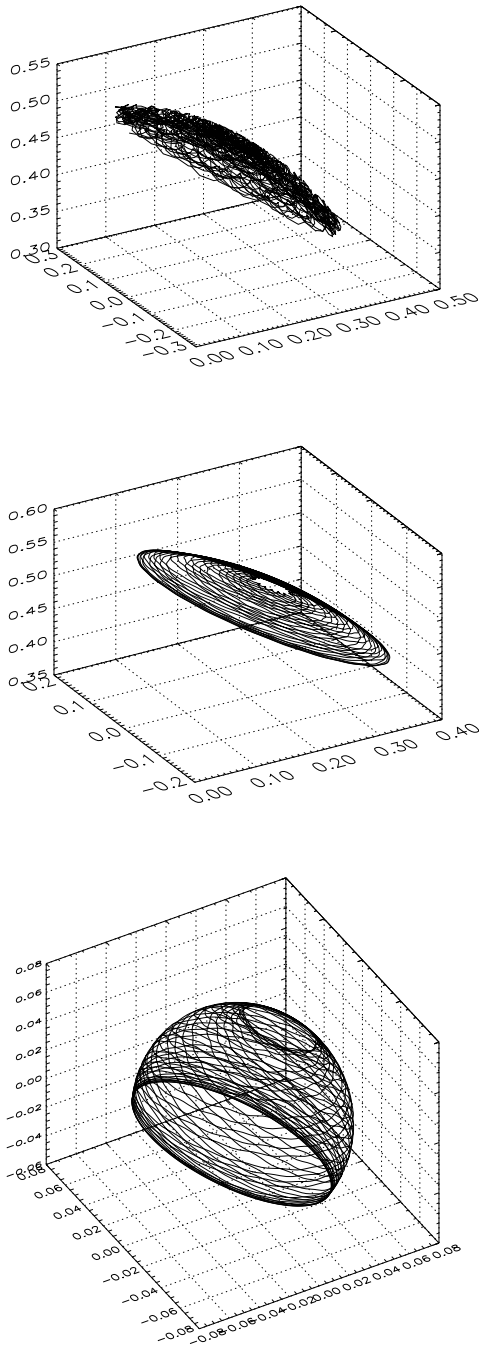


FIG. 10. The precession of the Newtonian angular momentum and spins for the orbit of fig. 9. Top: three-dimensional view of \vec{L}_N . Middle: three-dimensional view of the precession of \vec{S}_1 . Bottom: three-dimensional view of the precession of \vec{S}_2 .

VII. DISSIPATION

The emission of gravitational waves dissipates energy and angular momentum. The spins are not strongly affected by the loss of gravitational waves which carry away

orbital angular momentum and circularize the orbit as in fig. 11. The irregularity of a dissipative binary can be evaluated in terms of how many orbits the pair executes as it passes through the successive regions in the conservative system [24]. Figs. 11 and 12 illustrate the dissipative inspiral of a pair of maximally spinning black holes with $\beta = 1/3$. Fig. 12 shows the final group of cycles. The orbit begins fairly regular although the precession clearly modulates the waveform. As the signal enters the LIGO bandwidth, $r \sim 50m$ and the inclination angle is 14° . As the pair begins to leave the optimal LIGO bandwidth, when $r \sim 10m$, the inclination will have increased to 23° . The orbit becomes more irregular as the separation closes and the pair passes near the underlying conservative trajectory in fig. 6. Eventually the orbit nears the region of phase space described by fig. 9 and the motion appears highly irregular just before plunge.

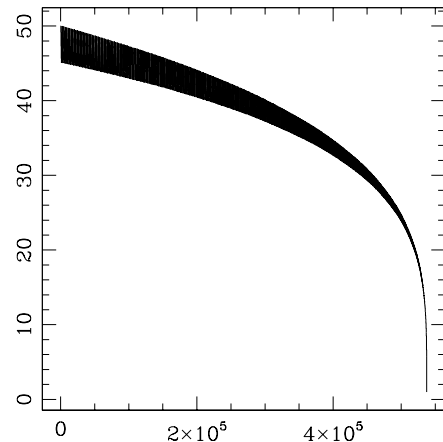


FIG. 11. The radius in units of r/m versus time in units of t/m for a dissipative BH/BH binary with $\beta = 1/3$.

The pair executes about 397 orbits for the range shown: over 250 orbits between $r \sim 50m$ and $r \sim 30m$, about 89 orbits between $r \sim 30m$ and $r \sim 20m$ and about 37 more down to $r \sim 10m$ and only about 6 or so orbits below $r \sim 10m$ before merger. The lighter object precesses ~ 15 times while the heavier object precesses ~ 7 times. The waveform is shown in the uppermost panel of fig. 13 while the lower panel shows the waveform of a nonspinning pair with otherwise identical initial conditions. The rapidly spinning pair takes about 397 cycles from $r \sim 50m$ to merger while a nonspinning pair takes about 370 over the same range. The number of additional cycles due to spin corresponds to roughly twice the total number of precessions in agreement with the results of Refs. [11,12].

Judging from fig. 13, a regular precession is modulating the amplitude and phase in a predictable way for $r \sim 50m$. Given unlimited access to theoretical templates, matched filtering could in principle glean a confident signal, at least until the pair drew closer than $r \sim 30m - 25m$. For the last $\mathcal{O}(50)$ orbits, right in

the optimal LIGO frequency range, the modulation becomes increasingly irregular. Since matched filtering relies on the template remaining in phase with the data for many cycles, one might hope that a disruption of the last few cycles would not be serious. Many authors have already argued for the use of other methods at these close separations (see [17] and the references therein). However, others have argued [25] that these last few orbits are heavily weighted and therefore critical for a successful detection. More important than the visually obvious amplitude modulation the precession modulates the gravitational wave frequency. A frequency space analysis is still required to determine if the modulation inhibits detectability of such irregular waves.

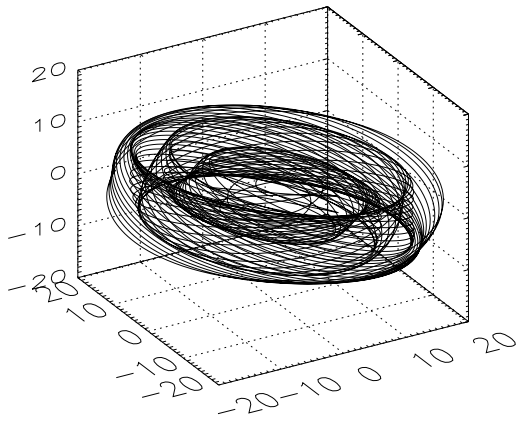


FIG. 12. Coalescing orbit with radiative reaction for $\beta = 1/3$. The last group of orbits before plunge.

On a more eccentric trajectory, the pair executed 170 orbits between $r \sim 50m$ and $r \sim 20m$ (bearing in mind the orbit is eccentric so these numbers are loose estimates), about 30 – 50 orbits between $r \sim 20m$ and $r \sim 10m$ and again only about 5 orbits below $r \sim 10m$ before merger.

A typical BH/NS pair with $\beta = 1.4/10$ will enter the LIGO bandwidth at an $r \lesssim 80m$. Giving the black hole a spin of $S_1 = m_1^2$ and the neutron star a spin of $S_2 = 0.7m_2^2$ (a period of $P \sim 10^{-3}$ s), the angle subtended by the orbital plane is $\sim 20^\circ$ if both spins are offset from \vec{L}_N by 45° when the gravitational wave frequency is $f \sim 10$ Hz and opens to $\sim 30^\circ$ when $f \sim 100$ Hz at $r \lesssim 15m$. Taking an orbit with a slight initial eccentricity, there is evidence of irregular motion for $r \lesssim 40m$ with the most prominent irregular modulation of the gravitational wave for the last couple of hundred or so orbits below $r \lesssim 30m$.

VIII. SUMMARY

A typical stellar mass BH/BH binary is shown to exhibit irregular precession of the orbital plane during the last $\mathcal{O}(30 - 50)$ orbits before merger. The dependence of the precessional motion was tested as a function of three parameters:

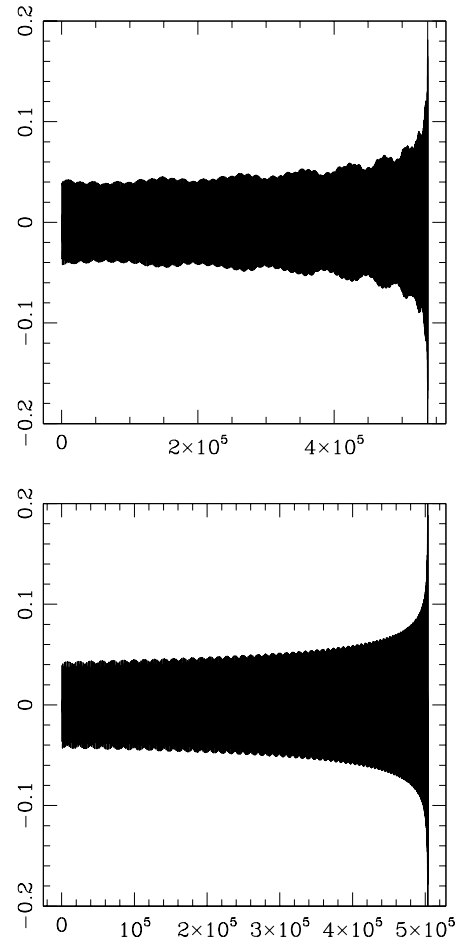


FIG. 13. Top: The waveform for the coalescing orbit of figs. 11 12. Bottom: For comparison, the waveform for an orbit with no spins but otherwise identical initial conditions.

- $\beta = m_2/m_1$: As was already known, the mass ratio determines the thickness of the band occupied by the precessing orbit [11,12]. A ratio of $\beta = 1/3$ is small enough for precession to modulate observable gravitational waves. The mass ratio may also determine the radius at which chaotic resonances occur by effecting the relative orbital and spin frequencies.

- eccentricity: Large eccentricity does not enhance irregular motion and may in fact suppress irregularities if very large. However, the usual relativistic precession of an elliptic orbit in the plane becomes superposed on the precession of the orbital plane. This combination, though not an indication of chaos, does lead to a compli-

cated modulation of the gravitational wave signal.

- spin magnitudes: The transition to chaos occurs as the spin magnitudes and misalignments are increased. There can be chaotic motion even when only one body spins. If it is a light companion spinning, then the magnitude of the spin has to be larger than maximal [1]. If it is the heavier object, then chaos can occur for rapid but physically allowed black hole spins (and then the motion will tend to be more irregular for modest eccentricities and smaller radial separations). For a given eccentricity and radial separation, a transition to chaos can occur as the spin of the companion is increased.

It is reasonable to conclude for a typical stellar mass BH/BH system that if the primary black hole spins rapidly, the orbital plane will precess unpredictably for the final few $\mathcal{O}(25)$ orbits. If both black holes spin, then the final $\mathcal{O}(30 - 50)$ cycles or more could be marked by unpredictable precession.

The most pressing question remains, will irregular orbits of coalescing binaries hinder observations? A detailed study of the modulated gravitational wave is needed. A conjecture is that an erratic precession of the orbital plane will result in an erratic frequency or phasing of the gravitational wave but will not alter the total number of cycles much. If this conjecture is fair, observations in the chaotic regime may be salvaged with a modification of the matched filtering method. As direct detections become more acute, we can aspire to watch the transition from regular to irregular motion. We might then witness the signature nonlinearity of general relativity determine the fate of chaotic binaries.

I am grateful to V. Kalogera, V. Kaspi, S. Portegies Zwart and F. Rasio for sharing their expertise. I want to especially thank J.D. Barrow, M. Bucher, E. Bertschinger, E. Copeland, N.J. Cornish, P. Ferreira, L. Grischuk, S.A. Hughes, R. O'Reilly, and B.S. Sathyaprakash for their insightful comments and support. I also want to thank the theoretical physics group at Imperial College for their hospitality. This work is supported by PPARC.

- [7] J. Levin, Phys. Rev. D. **60** 64015 (1999).
- [8] S.F. Portegies-Zwart and S.L. McMillan, astro-ph/9910061; astro-ph/9912022.
- [9] V. Kalogera, astro-ph/9911417.
- [10] For reviews on gravitational wave astronomy see K.S. Thorne, gr-qc/9704042; B.F. Schutz, Class. Quant. Grav. **16** A131 (1999). L.P. Grishchuk, V.M. Lipunov, K.A. Postnov, M.E. Prokhorov and B.S. Sathyaprakash astro-ph/0008481.
- [11] T.A. Apostolatos, C. Cutler, G.J. Sussman, and K.S. Thorne, Phys. Rev. D **15** 6274 (1994).
- [12] L. Kidder, Phys. Rev. D. **52** 821 (1995).
- [13] L. Blanchet and T. Damour, Ann. Inst. Henri Poincaré A, **50** 377 (1989); T. Damour and B.R. Iyer, Ann. Inst. Henri Poincaré **54** 115 (1991).
- [14] L.E. Kidder, C.M. Will and A.G. Wiseman, Phys. Rev. D **47** 3281 (1993).
- [15] J. Levin, R. O'Reilly, and E.J. Copeland, Phys. Rev. D **62** (2000) 024023.
- [16] L.S. Finn and D.F. Chernoff, Phys. Rev. D. **47** 2198 (1993).
- [17] S. A. Hughes, comment to appear in Phys. Rev. Lett..
- [18] N.J. Cornish, Proceedings of the Eighth Marcel Grossmann Meeting, Jerusalem, June 1992 gr-qc/9709036; also see gr-qc/9602054.
- [19] N.J. Cornish and J.J. Levin, Phys. Rev. Lett. **78** 998 (1997); Phys. Rev. D. **55** 7489 (1997).
- [20] T. Damour and N. Deruelle, C.R. Acad. Sci. Paris **293** 537 (1981); **293** 877 (1981); L.P. Grishchuk and S.M. Kopejkin, contribution to *Relativity in Celestial Mechanics and Astrometry*, ed J. Kovalevsky and V.A. Brumberg (Reidel, Dordrecht, 1986), p. 19.
- [21] L.E. Kidder, C.M. Will, and A.G. Wiseman, Phys. Rev. D **47** 4183 (1993).
- [22] A. J. Lichtenberg & M. A. Lieberman, *Regular and chaotic dynamics*, (Springer-Verlag, New York, 1992).
- [23] E. Ott, *Chaos in dynamical systems*, (Cambridge University Press, Cambridge, 1993).
- [24] see also the comment by N.J. Cornish to be published in Phys. Rev. Lett..
- [25] R.P. Croce, Th. Demma, V. Pierro, I.M. Pinto, D. Churches, and B.S. Sathyaprakash, gr-qc/0008059.

-
- [1] S. Suzuki and K. Maeda, Phys. Rev. D. **55** 4848 (1997).
 - [2] J. Levin, Phys. Rev. Lett. **84** 3515 (2000).
 - [3] G. Contopoulos, Proc. R. Soc. **A431** 183 (1990); Proc. R. Soc. **A435** 551 (1990).
 - [4] L. Bombelli and E. Calzetta, Class. Quantum. Grav. **9** 2573 (1992).
 - [5] C. P. Dettmann, N. E. Frankel and N. J. Cornish, Phys. Rev. D **50**, R618 (1994); Fractals, **3**, 161 (1995).
 - [6] N.J. Cornish and N.E. Frankel, Phys. Rev. D **56** 1903 (1997).

APPENDIX A: 2PN EQUATIONS OF MOTION

In the notation of Ref. [12], the center of mass equations of motion in harmonic coordinates are

$$\ddot{\mathbf{r}} = \vec{\mathbf{a}}_{\text{PN}} + \vec{\mathbf{a}}_{\text{SO}} + \vec{\mathbf{a}}_{\text{SS}} + \vec{\mathbf{a}}_{\text{RR}} \quad (\text{A1})$$

with $\vec{\mathbf{r}} = r\hat{\mathbf{r}}$. The right hand side is the sum of the contributions to the relative acceleration from the Post-Newtonian (PN) expansion, the spin-orbit (SO) and spin-spin (SS) coupling and from the radiative reaction (RR). The explicit terms are quoted from Ref. [12]. The following notation is used: $\vec{\mathbf{v}} = d\vec{\mathbf{r}}/dt$, $\hat{\mathbf{n}} \equiv \vec{\mathbf{r}}/r$, $\mu \equiv m_1 m_2 / m$, $\eta \equiv \mu / m$, $\delta m \equiv m_1 - m_2$, $\vec{\mathbf{S}} \equiv \vec{\mathbf{S}}_1 + \vec{\mathbf{S}}_2$, and $\vec{\mathbf{\Delta}} \equiv m(\vec{\mathbf{S}}_2/m_2 - \vec{\mathbf{S}}_1/m_1)$. The $\vec{\mathbf{a}}_{\text{PN}} = \vec{\mathbf{a}}_{\text{N}} + \vec{\mathbf{a}}_{1\text{PN}} + \vec{\mathbf{a}}_{2\text{PN}}$ with

$$\vec{\mathbf{a}}_{\text{N}} = -\frac{m}{r^2}\hat{\mathbf{n}}, \quad (\text{A2})$$

$$\vec{\mathbf{a}}_{1\text{PN}} = -\frac{m}{r^2} \left\{ \hat{\mathbf{n}} \left[(1 + 3\eta)v^2 - 2(2 + \eta)\frac{m}{r} - \frac{3}{2}\eta\dot{r}^2 \right] - 2(2 - \eta)\dot{r}\vec{\mathbf{v}} \right\}, \quad (\text{A3})$$

$$\begin{aligned} \vec{\mathbf{a}}_{2\text{PN}} = & -\frac{m}{r^2} \left\{ \hat{\mathbf{n}} \left[\frac{3}{4}(12 + 29\eta) \left(\frac{m}{r}\right)^2 + \eta(3 - 4\eta)v^4 + \frac{15}{8}\eta(1 - 3\eta)\dot{r}^4 \right. \right. \\ & \left. \left. - \frac{3}{2}\eta(3 - 4\eta)v^2\dot{r}^2 - \frac{1}{2}\eta(13 - 4\eta)\frac{m}{r}v^2 - (2 + 25\eta + 2\eta^2)\frac{m}{r}\dot{r}^2 \right] \right. \\ & \left. - \frac{1}{2}\dot{r}\vec{\mathbf{v}} \left[\eta(15 + 4\eta)v^2 - (4 + 41\eta + 8\eta^2)\frac{m}{r} - 3\eta(3 + 2\eta)\dot{r}^2 \right] \right\}, \end{aligned} \quad (\text{A4})$$

The radiative reaction term is due to terms to 5/2PN order and can be expressed as

$$\vec{\mathbf{a}}_{\text{RR}} = \frac{8}{5}\eta\frac{m^2}{r^3} \left\{ \dot{r}\hat{\mathbf{n}} \left[18v^2 + \frac{2}{3}\frac{m}{r} - 25\dot{r}^2 \right] - \vec{\mathbf{v}} \left[6v^2 - 2\frac{m}{r} - 15\dot{r}^2 \right] \right\}, \quad (\text{A5})$$

The spin-orbit acceleration is

$$\vec{\mathbf{a}}_{\text{SO}} = \frac{1}{r^3} \left\{ 6\hat{\mathbf{n}}[(\hat{\mathbf{n}} \times \vec{\mathbf{v}}) \cdot (2\vec{\mathbf{S}} + \frac{\delta m}{m}\vec{\mathbf{\Delta}})] - [\vec{\mathbf{v}} \times (7\vec{\mathbf{S}} + 3\frac{\delta m}{m}\vec{\mathbf{\Delta}})] + 3\dot{r}[\hat{\mathbf{n}} \times (3\vec{\mathbf{S}} + \frac{\delta m}{m}\vec{\mathbf{\Delta}})] \right\}. \quad (\text{A6})$$

and the spin-spin acceleration is

$$\vec{\mathbf{a}}_{\text{SS}} = -\frac{3}{\mu r^4} \left\{ \hat{\mathbf{n}}(\vec{\mathbf{S}}_1 \cdot \vec{\mathbf{S}}_2) + \vec{\mathbf{S}}_1(\hat{\mathbf{n}} \cdot \vec{\mathbf{S}}_2) + \vec{\mathbf{S}}_2(\hat{\mathbf{n}} \cdot \vec{\mathbf{S}}_1) - 5\hat{\mathbf{n}}(\hat{\mathbf{n}} \cdot \vec{\mathbf{S}}_1)(\hat{\mathbf{n}} \cdot \vec{\mathbf{S}}_2) \right\}. \quad (\text{A7})$$

1. Constants of the Motion

$$E = E_{\text{PN}} + E_{\text{SO}} + E_{\text{SS}}, \quad (\text{A8})$$

where $E_{\text{PN}} = E_{\text{N}} + E_{1\text{PN}} + E_{2\text{PN}}$ and

$$E_{\text{N}} = \mu \left\{ \frac{1}{2}v^2 - \frac{m}{r} \right\}, \quad (\text{A9})$$

$$E_{1\text{PN}} = \mu \left\{ \frac{3}{8}(1 - 3\eta)v^4 + \frac{1}{2}(3 + \eta)v^2\frac{m}{r} + \frac{1}{2}\eta\frac{m}{r}\dot{r}^2 + \frac{1}{2}\left(\frac{m}{r}\right)^2 \right\}, \quad (\text{A10})$$

$$\begin{aligned} E_{2\text{PN}} = & \mu \left\{ \frac{5}{16}(1 - 7\eta + 13\eta^2)v^6 - \frac{3}{8}\eta(1 - 3\eta)\frac{m}{r}\dot{r}^4 + \frac{1}{8}(21 - 23\eta - 27\eta^2)\frac{m}{r}v^4 \right. \\ & + \frac{1}{8}(14 - 55\eta + 4\eta^2)\left(\frac{m}{r}\right)^2 v^2 + \frac{1}{4}\eta(1 - 15\eta)\frac{m}{r}v^2\dot{r}^2 - \frac{1}{4}(2 + 15\eta)\left(\frac{m}{r}\right)^3 \\ & \left. + \frac{1}{8}(4 + 69\eta + 12\eta^2)\left(\frac{m}{r}\right)^2 \dot{r}^2 \right\}, \end{aligned} \quad (\text{A11})$$

$$E_{SO} = \frac{1}{r^3} \vec{\mathbf{L}}_{\mathbf{N}} \cdot \left(\vec{\mathbf{S}} + \frac{\delta m}{m} \vec{\Delta} \right), \quad (\text{A12})$$

$$E_{SS} = \frac{1}{r^3} \left\{ 3 \left(\hat{\mathbf{n}} \cdot \vec{\mathbf{S}}_1 \right) \left(\hat{\mathbf{n}} \cdot \vec{\mathbf{S}}_2 \right) - \left(\vec{\mathbf{S}}_1 \cdot \vec{\mathbf{S}}_2 \right) \right\}. \quad (\text{A13})$$

The total angular momentum is given by

$$\vec{\mathbf{J}} = \vec{\mathbf{L}} + \vec{\mathbf{S}}, \quad (\text{A14})$$

where

$$\vec{\mathbf{L}} = \vec{\mathbf{L}}_{\mathbf{PN}} + \vec{\mathbf{L}}_{\mathbf{SO}} \quad (\text{A15})$$

with $\vec{\mathbf{L}}_{\mathbf{PN}} = \vec{\mathbf{L}}_{\mathbf{N}} + \vec{\mathbf{L}}_{1\mathbf{PN}} + \vec{\mathbf{L}}_{2\mathbf{PN}}$ and

$$\vec{\mathbf{L}}_{\mathbf{N}} \equiv \mu (\vec{\mathbf{r}} \times \vec{\mathbf{v}}), \quad (\text{A16})$$

$$\vec{\mathbf{L}}_{1\mathbf{PN}} = \vec{\mathbf{L}}_{\mathbf{N}} \left\{ \frac{1}{2} v^2 (1 - 3\eta) + (3 + \eta) \frac{m}{r} \right\}, \quad (\text{A17})$$

$$\begin{aligned} \vec{\mathbf{L}}_{2\mathbf{PN}} = \vec{\mathbf{L}}_{\mathbf{N}} \left\{ \frac{3}{8} (1 - 7\eta + 13\eta^2) v^4 - \frac{1}{2} \eta (2 + 5\eta) \frac{m}{r} \dot{r}^2 \right. \\ \left. + \frac{1}{2} (7 - 10\eta - 9\eta^2) \frac{m}{r} v^2 \right. \\ \left. + \frac{1}{4} (14 - 41\eta + 4\eta^2) \left(\frac{m}{r} \right)^2 \right\}, \end{aligned} \quad (\text{A18})$$

and

$$\begin{aligned} \vec{\mathbf{L}}_{\mathbf{SO}} = \frac{\mu}{m} \left\{ \frac{m}{r} \hat{\mathbf{n}} \times \left[\hat{\mathbf{n}} \times \left(3\vec{\mathbf{S}} + \frac{\delta m}{m} \vec{\Delta} \right) \right] \right. \\ \left. - \frac{1}{2} \vec{\mathbf{v}} \times \left[\vec{\mathbf{v}} \times \left(\vec{\mathbf{S}} + \frac{\delta m}{m} \vec{\Delta} \right) \right] \right\}. \end{aligned} \quad (\text{A19})$$